Modeling Earth Systems and Environment (2025) 11:201
https://doi.org/10.1007/s40808-025-02375-2

ORIGINAL ARTICLE

Mathematical insights into chaos in fractional-order fishery model

Zakirullah[1] · Chen Lu[1] · Liang Li[1] · Kamal Shah[2] · Bahaaeldin Abdalla[2] · Thabet Abdeljawad[3,2,5,4]

Received: 17 January 2025 / Accepted: 6 March 2025 / Published online: 3 April 2025

Abstract

This study investigates the dynamics of a fractional-order model applied to fishery management to better illustrate the behavior of fish populations over time in a two-zone aquatic environment. The zones consist of unreserve and reserve zones prohibited from fishing. Initially, an integer-order nonlinear differential equation model was modified to fractional order in the Caputo sense modified intrinsic growth rate. Subsequently, the models are analyzed for positivity, boundedness, existence, and uniqueness, and stability analysis within the framework of the Caputo derivative order. The key parameters fishing mortality (ρ) and harvesting (Λ) allowed a detailed exploration of population growth and stability under various harvesting scenarios. The model is numerically solved using the Adam–Bashforth scheme with the Caputo derivatives. This method accounts for fractional order derivatives and provides an efficient numerical solution for nonlinear systems that are commonly observed in biological processes. Numerical simulations, varying the fractional order of the Caputo derivative, examine the impact of model parameters on system dynamics and control. In the fractional case, we establish sufficient conditions to guarantee the model's uniqueness and existence. An analysis of the dynamics of the system under various parameter settings and under different conditions which is potentially significant for understanding the complex behaviors of diverse biological systems. With the different input factors of the system, a novel numerical technique is presented for the chaotic and dynamic behaviour of the proposed model. Our analysis also shows that fractional order has an impact on the proposed system fishery model. Through numerical simulations, the most critical input parameters are highlighted and control interventions are suggested for policy makers to consider.

Keywords Fractional order mathematical fishery model · Chaos · Dynamics · Numerical results

✉ Zakirullah
zakirullahbzt@gmail.com

✉ Thabet Abdeljawad
tabdeljawad@psu.edu.sa

Chen Lu
luchensunshine@163.com

Liang Li
plum.liliang@gmail.com; plum_liliang@uestc.edu.cn

Kamal Shah
kamalshah408@gmail.com

Bahaaeldin Abdalla
babdallah@psu.edu.sa

[1] School of Mathematical Sciences, University of Electronic Science and Technology of China, Chengdu 611731, China

[2] Department of Mathematics and Sciences, Prince Sultan University, Riyadh 11586, Saudi Arabia

[3] Department of Mathematics, Saveetha School of Engineering, Saveetha Institute of Medical and Technical Sciences, Saveetha University, Chennai, Tamil Nadu 602105, India

[4] Department of Mathematics and Applied Mathematics, School of Science and Technology, Sefako Makgatho Health Sciences University, Ga-Rankuwa, South Africa

[5] Department of Medical Research, China Medical University, Taichung 40402, Taiwan

Introduction

Environmental impact of human activities has been widely recognized in recent years, including irreversible species losses, habitat destruction, and climate change. In population dynamics, it is described how population levels change over time. In order to understand these changes, predator–prey relationships are crucial for many species. The human population requires sustenance and energy in order to grow and develop, and animals need food in order to survive. Considering its broad relevance and practicality, the interdependency between predator and prey plays an essential role in ecology. The fishery resources are vital to maintaining a balanced ecosystem, as a significant portion of the population earns their living through fishing. To investigate where fisheries resources are dynamic in two fishing zones with human harvesting efforts and in the presence of predators with Crowley Martin functional response (Dasumani et al. 2024; Maurya et al. 2025; Yoshioka 2025). Environmental issues such as air and water pollution, overexploitation of marine ecosystems, and conserving biodiversity have attracted the attention of the public, stakeholders. Keeping, conserving, and managing aquatic and coastal resources are therefore important. Managing and controlling complex and multi-faceted dynamics and interactions between humans, production activities, and the environment is a crucial component of sustainable development. It is crucial to understand these interactions in order to promote sustainable development (Li et al. 2024; Maiti and Dubey 2017). Management of natural resources, including fishing, requires strategic planning, exploitation, and conservation that is sustainable for humans and the environment. Ecological integrity depends on resource management. In order to control such systems, it is crucial to understand how they evolve.

Human activities such as fishing are restricted and regulated in a marine protected area. The prohibition of fishing promotes sustainable fishing by allowing fish populations to recover from overfishing. Increasing fish spillover populations in neighboring areas can sometimes be demonstrated in support of reserved areas (Broadbridge et al. 2022). Fish species' survival depends on the ecological fitness of these zones for reproduction and size relative to fish mobility. Higher mobility and a low population density explain why spillover occurs more frequently for predator species than for herbivores (Weigel et al. 2014). In the 21st century, scenarios have evolved from tactical and simplistic to being dynamic simulations, which involve interacting species, environmental variability, and integrating with eco-economic optimization software (McClanahan et al. 2011). Control variables, including catch limits and reserved dimensions, can be managed with mathematical models that integrate a variety of information, such as fishers' experiences, field data on fish locations, movements, and behaviors, and statistical correlations. Species with more mobility are likely to wander into unprotected waters, so mathematical models consistently show that reserved areas are less effective for protecting them (e.g., Grüss 2014; Gerber et al. 2003).

Recent research has focused on using fractional calculus in mathematical modeling. Researchers have frequently applied the concepts of fractional calculus to study various real world problems (Khan et al. 2019; Paul et al. 2024; Mahmoud et al. 2020; Adel et al. 2024; Diallo et al. 2025). The study of fractional differential equations (FDEs) has drawn the attention of researchers from a variety of scientific and professional fields. Here, we remark that researchers have contributed significantly to the understanding of marine ecosystem dynamics and the evaluation of conservation strategies' effectiveness, etc by using fractional order models (Broadbridge et al. 2022; Weigel et al. 2014; Biswas et al. 2017). Standard mathematical models of integer-order derivatives, including non-linear systems, have significant limits in most cases. In classical differential operators, rate of change is assessed by using a limited set of two points. It is a genuine limitation. As a result, other methodologies have developed such as fractional differential operators that carry both singular and non-local kernels (Dasumani et al. 2024; Paul et al. 2023a, b). A fractional-order derivative provided a more accurate method of modeling complex systems than a traditional integer-order derivative. It is noteworthy that fractional-order models exhibit the memory effect, which classical models cannot capture because fractional operators have numerous properties (Buxton et al. 2014). Using fractional derivatives, we can capture hereditary properties and memory in dynamic systems, such as ecological and biological processes, including fishery dynamics. Furthermore, fractional-order derivatives allow us to uncover and analyze chaotic behavior within the system. The model provides a more comprehensive and realistic representation of the fishery system, leading to insights that are difficult to capture with traditional integer-order models. Thus, fractional-order derivatives are not arbitrary, but rooted in the necessity to represent the fundamental complexity of ecological processes.

Recent research demonstrates that fractional-order models comprehend complex physical events more accurately and deeply than integer-order. Their characteristics and memory-describing abilities play a role in this. An extension of conventional calculus is fractional calculus (Khan et al. 2023, 2024). There has been a growing popularity of fractional-order differential equations (FDEs) in a wide variety of fields such as control theory, engineering,

economics, and finance due to their higher degree of freedom and properties than integer-order differential equations (IDEs) (Lassong et al. 2024; Paul et al. 2024). Fractional-order derivatives have recently attracted the attention of many researchers interested in modeling real-world problems. Derivatives have been successfully applied to analyze and understand the nuanced dynamics of real-life problems (Ali et al. 2023; Li et al. 2011).

Recently, the Liouville–Caputo fractional-order derivatives (LC), the Caputo–Fabrizio fractional-order derivatives (CF), and others have been applied to mathematical models. In addition, a few mathematicians have applied the fractional-order derivative to social problems. Fractional differential equations offer information between two integer values, unlike conventional integer differential equations. The Caputo differential operator was used to investigate a fractional model of SM addiction. Mathematical models can be used to model a wide range of biological problems and analyze complex systems using fractional techniques. In order to understand fractional-order models, we recommend some references for more details theory, analysis and numerical investigations (Milici et al. 2018; Podlubny 1999; Yadav et al. 2019; Wang 2013).

Additionally, this paper is organized as follows: Section "Basic definitions" contains the essential definitions. The formulation of the model is detailed in Section "Formulation of model" with modified intrinsic growth rates in unreserved and reserved areas. Positivity, boundness, existence, and uniqueness are discussed in detail in Section "Positivity, boundness, existence, and uniqueness." The stability analysis and the equilibrium points are illustrated in Section "Stability analysis of steady states". The proposed technique for solving the model is highlighted in Section "Numerical method". Section "Numerical simulations of the fractional model" presents the numerical results of the work using the Adam–Bashforth scheme with the Caputo derivatives, and the conclusion for the work is provided in Section "Conclusion".

Basic definitions

Here are some definitions for these basic concepts (Milici et al. 2018; Podlubny 1999; Yadav et al. 2019).

Definition 2.1 The Caputo derivative of fractional order ξ of the function $y \in C[0,T]$ is given by

$$ {}^{C}\mathcal{D}_{t}^{\xi} y(t) = \begin{cases} \dfrac{1}{\Gamma(1-\xi)} \displaystyle\int_0^t (t-\tau)^{-\xi} \frac{dy}{d\tau} d\tau, & \text{if } \xi \in (0,1), \\ \dfrac{dy}{dt}, & \text{if } \xi = 1. \end{cases} \tag{1} $$

Further, the Riemann–Liouville fractional order ($\xi \in (0,1]$) integration of function y is defined by

$$ {}^{C}\mathcal{I}_{t}^{\xi} y(t) \frac{1}{\Gamma(\xi)} \int_0^t (t-\tau)^{\xi-1} y(\tau) d\tau. \tag{2} $$

Definition 2.2 The two parameters Mittag–Lefer function $E_{\xi,\xi_1}(t)$ is defined by

$$ E_{\xi,\xi_1}(t) = \Sigma_{n=0}^{\infty} \frac{t^n}{\Gamma(\xi n + \xi_1)}, \ \xi, \xi_1 > 0, \tag{3} $$

which further satisfies the following property given as

$$ E_{\xi,\xi_1}(y) = y E_{\xi,\xi+\xi_1}(y) + \frac{1}{\Gamma(\xi_1)}. \tag{4} $$

Definition 2.3 The Laplace transform of the function $t^{\xi_1-1} E_{\xi,\xi_1}(\pm\varepsilon\xi)$ is defined as follows:

$$ \pounds[t^{\xi_1-1} E_{\xi,\xi_1}(\pm\varepsilon\xi)] = \frac{s^{\xi-\xi_1}}{s^{\xi} \pm \varepsilon\xi}. \tag{5} $$

Hypothesis 1 Postulate $g \in \mathcal{L}^{\infty}(\mathcal{R}) \bigcap \mathcal{C}(\mathcal{R})$ and $\xi \in \mathcal{R}$, $n < \xi < n-1$. As a result, the condition below is met

1. ${}_{C}\mathcal{D}_{t}^{\xi} g(t) = g(t)$.
2. $\mathcal{J}_{C}^{\xi} \mathcal{D}_{t}^{\xi} g(t) = g(t) - \Sigma_{j=0}^{n-1} \frac{t^j}{j!} g^j(t)$.

Formulation of model

In this section of the paper, we construct ecological compartment models of fishery. In the context of a fishery resource comprising two distinct zones—a free fishing zone and a reserved area zone. The dynamics of a prey–predator system within a dual patch environment. One patch is open to both prey and predators, and the other is a refuge exclusively for prey. In this conceptualization, each area is considered as homogeneous. The prey sanctuary develops a protected area where fishing activities are strictly prohibited, in contrast to the open-access fishing domain of the unreserved zone outlined in Biswas et al. (2017). Furthermore, With these considerations, a logistic classical integer order modified model formulation can be developed based on the growth of fish populations in each

zone. Let's denote $\mathcal{U}(t)$ as the biomass density within the unreserved area and $\mathcal{V}(t)$ as the biomass density within the reserved area. Λ represents the total effort applied for harvesting the fish population in the unreserved area, and ρ is a coefficient representing fishing mortality. α and β are the intrinsic growth rates of the fish sub-populations inside the unreserved and reserved areas, respectively. γ and δ represent the rates of migration from the unreserved to the reserved area and from the reserved to the unreserved area, respectively. The modified intrinsic growth rates in unreserved and reserved areas are represented by α and β, respectively. So, the new parameters v, μ, κ and ε. The growth rate of the fish population in the unreserved area is represented as $\alpha = \mu v$, where v reflects biological factors, including the reproduction rate of fish and μ an account for environmental factors such as food availability or habitat conditions in this zone. Similarly, the growth rate of the fish population in the reserved area is represented as $\beta = \kappa\varepsilon$, where κ captures biological aspects like the species' reproductive capabilities,and ε refers to the environmental conditions in the refuge in the reserved zone. The system in the Caputo's sense is as follows:

$$\begin{aligned} {}^{C}\mathcal{D}_t^{\xi}\mathcal{U} &= \alpha\mathcal{U}\left(1-\frac{\mathcal{U}}{\Phi}\right) - \gamma\mathcal{U} + \mathcal{V}\delta - \rho\Lambda\mathcal{U}, \\ {}^{C}\mathcal{D}_t^{\xi}\mathcal{V} &= \beta\mathcal{V}\left(1-\frac{\mathcal{V}}{\Psi}\right) + \gamma\mathcal{U} - \mathcal{V}\delta, \end{aligned} \tag{6}$$

with the initial conditions $\mathcal{U}(t_0) = \mathcal{U}(0)$ and $\mathcal{V}(t_0) = \mathcal{V}(0)$.

Positivity, boundedness, existence, and uniqueness

The current section is further divided in some subsections.

Positivity and boundedness Ω

This subsection discusses the positive analysis and boundness of the model (6).

Theorem 4.1 *If $\mathcal{U}(t), \mathcal{V}(t) \geq 0$, then the solutions of $\mathcal{U}$ and $\mathcal{V}$ are positive. Suppose $\mathcal{U}(t)$ and $\mathcal{V}(t)$ are positive, then all solutions are positive for $t > 0$.*

Proof In (6), if the first equation is considered

$${}^{C}\mathcal{D}_t^{\xi}\mathcal{U}(t) = \alpha\mathcal{U}(t)\left(1-\frac{\mathcal{U}(t)}{\Phi}\right) - \gamma\mathcal{U}(t) + \mathcal{V}(t)\delta - \rho\Lambda\mathcal{U}, \tag{7}$$

implies that

$${}^{C}\mathcal{D}_t^{\xi}\mathcal{U}(t) + (\gamma + \rho\Lambda)\mathcal{U}(t) \geq 0. \tag{8}$$

Using the Laplace transform definition, the following results can be obtained

$$\begin{aligned} &\pounds[\ {}^{C}\mathcal{D}_t^{\xi}\mathcal{U}(t)] + \pounds[(\gamma + \rho\Lambda)\mathcal{U}(t)] \geq 0, \\ &s^u\mathcal{U}(s) - s^{u-1}\mathcal{U}(0) + (\gamma\mathcal{U}(t) + \rho\Lambda)\mathcal{U}(s) \geq 0, \\ &\mathcal{U}(s) \geq \frac{s^{u-1}}{(s^u + (\gamma + \rho\Lambda))}U(0). \end{aligned} \tag{9}$$

the inverse Laplace transform yields the following results,

$$\begin{aligned} \pounds^{-1}\{\mathcal{U}(s)\} &\geq \pounds^{-1}\left\{\frac{s^{u-1}}{s^u + \gamma + \rho\Lambda}\mathcal{U}(0)\right\}, \\ \mathcal{U}(t) &\geq K_{\xi,1}(-\gamma + \rho\Lambda)\mathcal{U}(0). \end{aligned} \tag{10}$$

Given that the quantities on the right-hand side are positive, it follows that $\mathcal{U} \geq 0$ for $t > 0$. Using a similar approach, given any non-negative initial values, $\mathcal{V}$ is greater than or equal to 0 for any $t > 0$. Thus, the solution remains in R_+^2 for all $t > 0$ with non-negative initial values. Next, we demonstrate that the fractional model solution is bounded.

Theorem 4.2 *The set $\Omega = \{(\mathcal{U}(t), \mathcal{V}(t)) \in R_2^2 : \hbar = \mathcal{U}(t) + \mathcal{V}(t) \preceq \frac{\theta}{\phi}\}$ is the region that attracts all solutions that initiate the positive quadrant's interior, where $\mathcal{U}(t)$ is a positive constant and $\theta = \frac{\Phi}{4\alpha}(\alpha - \phi - \rho\Lambda)^2 + \frac{\Psi}{4\beta}(\beta + \phi)^2$.*

Proof let $\hbar = \mathcal{U}(t) + \mathcal{V}(t)$ and $\phi > 0$ be constants; therefore, we obtain

$$\begin{aligned} {}^{C}\mathcal{D}_t^{\xi}\hbar(t) &= -\frac{\alpha\mathcal{U}(t)^2}{\Phi} + (\alpha - \phi - \rho\Lambda)^2\mathcal{U}(t)^2 \\ &\quad - \frac{\beta\mathcal{V}(t)^2}{\Psi} + (\beta + \phi)\mathcal{V}(t), \\ {}^{C}\mathcal{D}_t^{\xi}\hbar(t) &\leq \frac{\Phi}{4\alpha}(\alpha - \phi - \rho\Lambda)^2 + \frac{\Psi}{4\beta}(\beta + \phi)^2, \\ s^{\xi}\pounds\{\hbar(t)\} - s^{\xi-1}\hbar(0) &\leq \frac{\theta}{s\phi}, \\ \pounds\{\hbar(t)\} &\leq \frac{1}{s}\hbar(0) + \frac{1}{s^{\xi+1}}\frac{\theta}{\phi}. \end{aligned} \tag{11}$$

By letting $t \to \infty$, $\hbar \leq \frac{\theta}{\phi}$, which implies that $lim_{\to\infty} \sup \hbar = \frac{\theta}{\phi}$, indicating that Ω is bounded. Thus, this establishes the set Ω concept as required. Therefore, it can be concluded that the region is ecological feasible and well-posed in Ω. □

Existence and uniqueness

This subsection is dedicated to proving the existence and uniqueness of the solution of model (6). Consider Tas a negative real number and take $k = [0, T]$ into account. Define the set of all continuous functions on κ by $C_e^0\ (k)$ with the norm $\|\hbar\| = sup\{|\hbar(t)|, t \in k\}$. The initial conditions for the system (6) are as follows:

$$\begin{aligned} {}^{c}\mathcal{D}t^{\xi}\hbar(t) &= \Pi(t,\ \hbar(t)), 0<t<T<\infty, \\ (\mathcal{U}(0),\ \mathcal{V}(0)) &= (\mathcal{U}_0,\ \mathcal{V}_0). \end{aligned} \tag{12}$$

In this context, $\hbar(t) = (\mathcal{U}(t),\ \mathcal{V}(t))$ represents the compartments, and Π is a continuous function in the following way:

$$\begin{aligned} \Pi(t,\ \hbar(t)) &= \begin{pmatrix} \Pi_1(t,\mathcal{U}(t)) \\ \Pi_2(t,\ \mathcal{V}(t)) \end{pmatrix} \\ &= \begin{pmatrix} \alpha\mathcal{U}(t)(1-\frac{\mathcal{U}(t)}{\Phi}) - \gamma\mathcal{U}(t) + \mathcal{V}(t)\delta - \rho\Lambda\mathcal{U}(t) \\ \beta\mathcal{V}(t)(1-\frac{\mathcal{V}(t)}{\Psi}) + \gamma\mathcal{U}(t) - \mathcal{V}(t)\delta \end{pmatrix}. \end{aligned} \tag{13}$$

Using property from Hypothesis 1, we have

$$\begin{aligned} \mathcal{U}(t) &= \mathcal{U}_0 + \ell_i^{\xi}(\alpha\mathcal{U}(t)\left(1-\frac{\mathcal{U}(t)}{\Phi}\right) - \gamma\mathcal{U}(t) + \mathcal{V}(t)\delta - \rho\Lambda\mathcal{U}(t)), \\ \mathcal{V}(t) &= \mathcal{V}_0 + \ell_i^{\xi}(\beta\mathcal{V}(t)\left(1-\frac{\mathcal{V}(t)}{\Psi}\right) + \gamma\mathcal{U}(t) - \mathcal{V}(t)\delta). \end{aligned} \tag{14}$$

The Picard iterations recursive formulas lead as follows

$$\begin{aligned} \mathcal{U}_n(t) &= \frac{1}{\Gamma(\xi)}\int_0^t (t-\ell)^{\xi-1}\Pi_1(\ell,\mathcal{U}(\ell)_{n-1})d\ell, \\ \mathcal{V}_n(t) &= \frac{1}{\Gamma(\xi)}\int_0^t (t-\ell)^{\xi-1}\Pi_2((\ell,\mathcal{V}(\ell)_{n-1})d\ell, \end{aligned} \tag{15}$$

and

$$\begin{aligned} \mathcal{U}_{n-1}(t) &= \frac{1}{\Gamma(\xi)}\int_0^t (t-\ell)^{\xi-1}\Pi_1(\ell,\mathcal{U}(\ell)_{n-2})d\ell, \\ \mathcal{V}_{n-1}(t) &= \frac{1}{\Gamma(\xi)}\int_0^t (t-\ell)^{\xi-1}\Pi_1(\ell,\mathcal{U}(\ell)_{n-2})d\ell. \end{aligned} \tag{16}$$

The subtraction of two consecutive terms in the recursive formula is given by

$$\begin{aligned} \mathcal{U}_n(t) - \mathcal{U}_{n-1}(t) &= \frac{1}{\Gamma(\xi)}\int_0^t (t-\ell)^{\xi-1}\Pi_1((\ell,\mathcal{U}(\ell)_{n-1}) \\ &\quad - (\ell,\mathcal{U}(\ell)_{n-2}))d\ell, \\ \mathcal{V}_n(t) - \mathcal{V}_{n-1}(t) &= \frac{1}{\Gamma(\xi)}\int_0^t (t-\ell)^{\xi-1}\Pi_2((\ell,\mathcal{V}(\ell)_{n-1}) \\ &\quad - (\ell,\mathcal{V}(\ell)_{n-2}))d\ell. \end{aligned} \tag{17}$$

Thus, it follows that

$$\mathcal{U}_n(t) = \sum_{i-1}^{n}\chi_n(t), \mathcal{V}_n(t) = \sum_{i-1\psi n}^{n}\psi(t). \tag{18}$$

The definitive form of the I.V.P. Equation (12) can be articulated as follows:

$$\hbar(t) = \hbar(0) + \frac{1}{\Gamma(\xi)}\int_0^t (t-\ell)^{\xi-1}\Pi(\ell,\hbar(\ell))d\ell. \tag{19}$$

Lemma 4.2.1 *The vector $\Pi(t,\hbar(t))$ presented in (13) fulfill the well-known Lipschitz condition in the variable $\hbar$ on a set $[0,T]\times R_+^2$ with the Lipschitz constant. The notations that followed are analyzed . Since $\mathcal{U}(t)$, $\mathcal{V}(t)$ are non-negative bounded functions, there exist positive values $\varphi_1$and φ_2 such that $\|\mathcal{U}(t)\| \le \varphi_1, \|\mathcal{V}(t)\| \le \varphi_2$.*

Proof

$$\begin{aligned} \alpha^{\dagger} &= \max_{t\in[0,T]}|\alpha(t)|,\ \beta^{\dagger} = \max_{t\in[0,T]}|\beta(t)|, \\ \zeta_1 &= \left(\alpha^{\dagger} - \gamma - \rho\Lambda - \frac{\alpha^{\dagger}}{\Phi} + \delta\frac{\varphi_2}{\varphi_1}\right) \\ \varphi_1,\ \zeta_2 &= \left(\beta^{\dagger} - \delta - \frac{\beta^{\dagger}}{\Psi} + \gamma\frac{\varphi_1}{\varphi_2}\right)\varphi_2, \\ \mathfrak{x} &= \max\left(\left(\alpha^{\dagger} - \gamma - \rho\Lambda - \frac{\alpha^{\dagger}}{\Phi} + \delta\frac{\varphi_2}{\varphi_1}\right)\varphi_1,\right. \\ &\qquad \left.\left(\beta^{\dagger} - \delta - \frac{\beta^{\dagger}}{\Psi} + \gamma\frac{\varphi_1}{\varphi_2}\right)\right). \end{aligned}$$

Now, recursive inequalities are computed for differences (18) as follows

$$\begin{aligned}\chi_n(t) &= \|\mathcal{U}_n(t) - \mathcal{U}_{n-1}(t)\| \\ &= \left\| \frac{1}{\Gamma(\xi)} \int_0^t (t-\ell)^{\xi-1} \Pi_1((\ell, U(\ell)_{n-1}) - (\ell, U(\ell)_{n-2}))d\ell \right\|, \\ &\leq \zeta_1 t \|\mathcal{U}_{n-1}(t) - \mathcal{U}_{n-2}(t)\|, \\ &\leq \zeta_1 t \|\chi_{n-1}(t)\|. \end{aligned} \tag{20}$$

Similarly,

$$\begin{aligned}\psi(t) &= \|\mathcal{V}_n(t) - \mathcal{V}_{n-1}(t)\| \\ &= \left\| \frac{1}{\Gamma(\xi)} \int_0^t (t-\ell)^{\xi-1} \Pi_2((\ell, \mathcal{V}(\ell)_{n-1}) - (\ell, \mathcal{V}(\ell)_{n-2}))d\ell \right\|, \\ &\leq \zeta_2 t \|\mathcal{V}_{n-1}(t) - \mathcal{V}_{n-2}(t)\|, \\ &\leq \zeta_2 t \|\psi_{n-1}(t)\|. \end{aligned} \tag{21}$$

Combining all these we have

$$\|\Pi(t, \hbar_1(t)) - \Pi(t, \hbar_2(t))\| \leq \|\hbar_1(t) - \hbar_2(t)\|, \tag{22}$$

$$\begin{aligned}\mathfrak{X} = \max\Bigg(&\left(\alpha^{\dagger} - \gamma - \rho\Lambda - \frac{\alpha^{\dagger}}{\Phi} + \delta\frac{\varphi_2}{\varphi_1} \right)\varphi_1, \\ &\left(\beta^{\dagger} - \delta - \frac{\beta^{\dagger}}{\Psi} + \gamma\frac{\varphi_1}{\varphi_2} \right) \Bigg). \end{aligned} \tag{23}$$

□

Theorem 4.3 *Unique solution of* (12) *exists if the Leibniz condition* (23) *is satisfied and* $\frac{\mathfrak{X}}{\Gamma(\xi+1)}\Theta$.

Proof For the required result definition is considered as $\hbar(t) = \Theta(\hbar(t))$, where Θ is the Picard operator defined as: $\Theta : C_e^0(k,\ R_+^2) \longrightarrow C_e^0(k,\ R_+^2)$

$$\Theta(\hbar(t)) = \hbar(0) + \frac{1}{\Gamma(\xi)} \int_0^t (t-\ell)^{\xi-1} \Pi(\ell, \hbar(\ell))d\ell. \tag{24}$$

Which is also a second-kind Volterra equation. This leads to

$$\begin{aligned}\|\Theta(\hbar_1(t)) - \Theta(\hbar_2(t))\| &= \left\| \frac{1}{\Gamma(\xi)} \int_0^t (t-\ell)^{\xi-1} [\Pi(\ell, \hbar_1(\ell) - \Pi(\ell, \hbar_2(\ell))]d\ell \right\|, \\ &\leq \frac{1}{\Gamma(\xi)} \int_0^t (t-\ell)^{\xi-1} \|\Pi(\ell, \hbar_1(\ell) - \Pi(\ell, \hbar_2(\ell))\|d\ell, \\ &\leq \frac{1}{\Gamma(\xi)} \int_0^t (t-\ell)^{\xi-1} \|\hbar_1(\ell) - \hbar_2(\ell)\|d\ell, \\ &\leq \frac{\mathfrak{X}}{\Gamma(\xi+1)}\Theta. \end{aligned} \tag{25}$$

Therefore $\frac{\mathfrak{X}}{\Gamma(\xi+1)}\Theta < 1$, there is $\|\Pi(t, \hbar_1(t)) - \Pi(t, \hbar_2(t))\| \leq \|\hbar_1(t) - \hbar_2(t)\|$.

This indicates that the equation's problem has a unique solution. □

Stability analysis of steady states

Theorem 5.1 *The steady-state* $(\mathcal{U}^*, \mathcal{V}^*) = (0, 0)$ *is stable only if all eigenvalues for Jacobian matrix J have negative real parts. Otherwise, the system is unstable.*

Proof Suppose that the steady state $(\mathcal{U}^*, \mathcal{V}^*) = (0, 0)$ of the given system(6). The Jacobian matrix for the system is

$$J(\mathcal{U}, \mathcal{V}) = \begin{pmatrix} \alpha - \frac{2\alpha}{\Phi}\mathcal{U}^0 - \gamma - \rho\Lambda & \delta \\ \gamma & \beta - \frac{2\beta}{\Psi}\mathcal{V}^0 - \delta \end{pmatrix}.$$

At the steady state $J(\mathcal{U}, \mathcal{V}) = (0,\ 0)$, this simplifies to:

$$J(0,0) = \begin{pmatrix} \alpha - \gamma - \rho\Lambda & \delta \\ \gamma & \beta - \delta \end{pmatrix}.$$

To determine stability, J has the following eigenvalues as determined by its roots:

$$\begin{vmatrix} \alpha - \gamma - \rho\Lambda & 0 \\ 0 & \beta - \delta \end{vmatrix} = 0$$

The eigenvalues of the matrix J are:

$$\lambda_1 = -\gamma - \Lambda\rho + \alpha,$$
$$\lambda_2 = -\delta + \beta.$$

In the steady state, all eigenvalues are real and negative, determining the stability of the states; therefore, the steady state is stable based on the idea of the Routh-Hurwitz criterion.

Theorem 5.2 *The equilibrium point* $(\mathcal{U}^*,\ \mathcal{V}^*)$ *is globally asymptotically stable* (*GAS*).

Proof Consider the following Lyapunov function L related to the equilibrium point $(\mathcal{U}^*,\ \mathcal{V}^*)$:

$$L(t) = K_1\left(\mathcal{U} - \mathcal{U}^* - \mathcal{U}^* \ln\frac{\mathcal{U}}{\mathcal{U}^*}\right) + K_2\left(\mathcal{V} - \mathcal{V}^* - \mathcal{V}^* \ln\frac{\mathcal{V}}{\mathcal{V}^*}\right).$$

The Caputo fractional derivative of L with respect to time t implies:

$${}^{C}\mathcal{D}_t^{\xi} L(t) = K_1\left(1 - \frac{\mathcal{U}^*}{\mathfrak{U}}\right)^{C}\mathcal{D}_t^{\xi}\mathcal{U} + K_2\left(1 - \frac{\mathcal{V}^*}{\mathcal{V}}\right)^{C}\mathcal{D}t^{\xi}\mathcal{V},$$

leads to,

$$\begin{aligned}{}^{C}\mathcal{D}_t^{\xi} L(t) = &-\frac{\alpha}{\Phi}(\mathcal{U} - \mathcal{U}^*)^2 - \frac{1}{\Psi}\beta\frac{\gamma}{\delta}\frac{\mathcal{U}^*}{\mathcal{V}^*}(\mathcal{V} - \mathcal{V}^*) \\ &- \frac{1}{\mathcal{U}\mathcal{V}}\frac{\delta}{\mathcal{U}^*}(\mathcal{U}\mathcal{V}^* - \mathcal{V}\mathcal{U}^*). \end{aligned}$$

This demonstrates that ${}^{C}\mathcal{D}_{t}^{\xi}L(t)$ is negative, it follows by Lyapunov's direct method that the equilibrium point $(\mathcal{U}^{*}, \mathcal{V}^{*})$ is GAS.

Numerical method

The numerical tools outlined in Yadav et al. (2019), Wang (2013) for simulations. Following such a method, we introduced a novel numerical method that leverages the Caputo fractional derivative for discretizing differential equations. This approach has been used to obtain the numerical solution for system (6) with chaotic behavior.

Take into account the fractional differential equation referenced in definition

$$ {}^{C}\mathcal{D}_{t}^{\xi} = g(t, z(t)) = \frac{1}{\Gamma(\xi)} \int_{0}^{t} g(\ell, z(\ell))(t-\ell)^{\xi-1} d\ell. \tag{26}$$

Employing the fundamental theorem of calculus on Eq. (26) yields

$$ z(t) - z(0) = \frac{1}{\Gamma(\xi)} \int_{0}^{t} g(\ell, z(\ell))(t-\ell)^{\xi-1} d\lambda, \tag{27}$$

therefore, for $t = t_{m+1}$

$$ z(t_{m+1}) - z(0) = \frac{1}{\Gamma(\xi)} \int_{0}^{t_{m+1}} (t_{m+1}-t)^{\xi-1} g(t, z(t)) dt, \tag{28}$$

and

$$ z(t_{m}) - z(0) = \frac{1}{\Gamma(\xi)} \int_{0}^{t_{m}} (t_{m}-t)^{\xi-1} g(t, z(t)) dt. \tag{29}$$

By taking the difference between Eq. (28) and Eq. (29), the result is

$$\begin{aligned} z(t_{m+1}) =& z(t_{m}) + \frac{1}{\Gamma(\xi)} \int_{0}^{t_{m+1}} (t_{m+1}-t)^{\xi-1} g(t, z(t)), \\ &+ \frac{1}{\Gamma(\xi)} \int_{0}^{t_{m}} (t_{m}-t)^{\xi-1} g(t, z(t)) dt. \end{aligned} \tag{30}$$

Equation (30) can be expressed as

$$ z(t_{m+1}) = z(t_{m}) + \mathcal{A}_{\xi,1} + \mathcal{A}_{\xi,2} t, \tag{31}$$

where

$$ \mathcal{A}_{\xi,1} = \frac{1}{\Gamma(\xi)} \int_{0}^{t_{m+1}} (t_{m+1}-t)^{\xi-1} g(t, z(t)) dt$$

and

$$ \mathcal{A}_{\xi,2} = \frac{1}{\Gamma(\xi)} \int_{0}^{t_{m}} (t_{m}-t)^{\xi-1} g(t, z(t)) dt.$$

Lagrange interpolation allows the function $g(t, z(t))$ to be approximated as

$$\begin{aligned} p(t) &\simeq \frac{t-t_{m-1}}{t_{m}-t_{m-1}} g(t_{m}, z_{m}) + \frac{t-t_{m}}{t_{m-1}-t_{m}} g(t_{m-1}, z_{m-1}), \\ p(t) &= \frac{g(t_{m}, z_{m})}{h}(t-t_{m-1}) - \frac{g(t_{m-1}, z_{m-1})}{h}(t-t_{m}). \end{aligned}$$

This leads to

$$\begin{aligned} \mathcal{A}_{\xi,1} =& \frac{g(t_{m}, z_{m})}{h\Gamma(\xi)} \int_{0}^{t_{m+1}} (t_{m+1}-t)^{\xi-1}(t-t_{m-1}) dt - \frac{g(t_{m-1}, z_{m-1})}{h\Gamma(\xi)} \\ &\times \int_{0}^{t_{m+1}} (t_{m+1}-t)(t-t_{m}) dt, \\ \mathcal{A}_{\xi,1} =& \frac{g(t_{m}, z_{m})}{h\Gamma(\xi)} \int_{0}^{t_{m+1}} z^{\xi-1}(t_{m+1}-z-t_{m-1}) dy - \frac{g(t_{m-1}, z_{m-1})}{h\Gamma(\xi)} \\ &\times \int_{0}^{t_{m+1}} z^{\xi-1}(t_{m+1}-z-t_{m}) dy. \end{aligned}$$

Hence,

$$\begin{aligned} \mathcal{A}_{\xi,1} =& \frac{g(t_{m}, z_{m})}{h\Gamma(\xi)} \left\{ \frac{2ht_{m+1}^{\xi}}{\xi} - \frac{t_{m+1}^{\xi+1}}{\xi+1} \right\} \\ &- \frac{g(t_{m-1}, z_{m-1})}{h\Gamma(\xi)} \left\{ \frac{ht_{m+1}^{\xi}}{\xi} - \frac{t_{m+1}^{\xi+1}}{\xi+1} \right\}. \end{aligned} \tag{32}$$

Using a similar approach, we derive

$$\begin{aligned} \mathcal{A}_{\xi,2} =& \frac{g(t_{m}, z_{m})}{h\Gamma(\xi)} \int_{0}^{t_{m}} (t_{m}-t)^{\xi-1}(t-t_{m-1}) dt - \frac{(t_{m-1}, z_{m-1})}{h\Gamma(\xi)} \\ &\times \int_{0}^{t_{m}} (t_{m}-t)^{\xi-1}(t-t_{m}) dt, \\ \mathcal{A}_{\xi,2} =& \frac{g(t_{m}, z_{m})}{h\Gamma(\xi)} \int_{0}^{t_{m}} z^{\xi-1}(t_{m}-z-t_{m-1}) dy - \frac{g(t_{m-1}, z_{m-1})}{h\Gamma(\xi)} \frac{t_{m}^{\xi+1}}{\xi}, \\ \mathcal{A}_{\xi,2} =& \frac{g(t_{m}, z_{m})}{h\Gamma(\xi)} \left\{ \frac{ht_{m}^{\xi}}{\xi} - \frac{t_{m}^{\xi+1}}{\xi+1} \right\} + \frac{g(t_{m-1}, z_{m-1})}{h\Gamma(\xi+1)} t_{\xi}^{\xi+1}. \end{aligned} \tag{33}$$

Substitute Eq. (32) and Eq. (33) into Eq. (31), the approximate solution is formulated as

$$z(t_{m+1}) = z(t_m) + \frac{g(t_m, z_m)}{h\Gamma(\xi)}\left\{\frac{2ht_{m+1}^{\xi}}{\xi} - \frac{t_{m+1}^{\xi+1}}{\xi+1} + \frac{ht_m^{\xi}}{\xi} - \frac{t_m^{\xi+1}}{\xi+1}\right\} + \frac{g(t_{m-1}, z_{m-1})}{h\Gamma(\xi)}\left\{\frac{ht_{m+1}^{\xi}}{\xi} - \frac{t_{m+1}^{\xi+1}}{\xi+1} + \frac{t_m^{\xi}}{\xi+1}\right\}. \tag{34}$$

Theorem 6.1 *Let ${}^{\mathcal{C}}\mathcal{D}_t^{\xi} = g(t, z(t))$ is a fractional differential equation with g bounded, the numerical solution for $z(t)$ is expressed as*

$$z(t_{m+1}) = z(t_m) + \frac{g(t_m, z_m)}{h\Gamma(\xi)}\left\{\frac{2ht_{m+1}^{\xi}}{\xi} - \frac{t_{m+1}^{\xi+1}}{\xi+1} + \frac{ht_m^{\xi}}{\xi} - \frac{t_m^{\xi+1}}{\xi+1}\right\} + \frac{g(t_{m-1}, z_{m-1})}{h\Gamma(\xi)}\left\{\frac{ht_{m+1}^{\xi}}{\xi} - \frac{t_{m+1}^{\xi+1}}{\xi+1} + \frac{t_m^{\xi}}{\xi+1}\right\} + \mathcal{R}_m^{\xi}(t), \tag{35}$$

where $R_m^{\xi}(t) < \frac{h^{3+\xi}M}{12\Gamma(\xi+1)}\{(n+1)^{\xi} + n^2\}$.

By rearranging this system (6) as per the fundamental theorem of analysis, the next set of Eq. (6) for the G_i kernels are derived, where $\mathcal{K}_i = 1, 2$.

$$\begin{aligned}\mathcal{U}(t) - \mathcal{U}(0) &= \frac{1}{\Gamma(\xi)}\int_0^t \mathcal{K}_1(\ell, \mathcal{U}(t))(t-\ell)^{\xi-1}d\lambda,\\ \mathcal{V}(t) - \mathcal{V}(0) &= \frac{1}{\Gamma(\xi)}\int_0^t \mathcal{K}_2(\ell, \mathcal{V}(t))(t-\ell)^{\xi-1}d\lambda.\end{aligned} \tag{36}$$

Accordingly, at $t = t_{m+1}$

$$\begin{aligned}\mathcal{U}(t_{m+1}) - \mathcal{U}(0) &= \frac{1}{\Gamma(\xi)}\int_0^{t_{m+1}} (t_{m+1}-t)^{\xi-1} g(t, \mathcal{U}(t))dt,\\ \mathcal{V}(t_{m+1}) - \mathcal{V}(0) &= \frac{1}{\Gamma(\xi)}\int_0^{t_{m+1}} (t_{m+1}-t)^{\xi-1} g(t, \mathcal{V}(t))dt,\end{aligned} \tag{37}$$

and

$$\begin{aligned}\mathcal{U}(t_m) - \mathcal{U}(0) &= \frac{1}{\Gamma(\xi)}\int_0^{t_m} (t_m-t)^{\xi-1} g(t, \mathcal{U}(t))dt,\\ \mathcal{V}(t_m) - \mathcal{V}(0) &= \frac{1}{\Gamma(\xi)}\int_0^{t_m} (t_m-t)^{\xi-1} g(t, \mathcal{V}(t))dt.\end{aligned} \tag{38}$$

Taking Eq. (37) and subtracting Eq. (38) results in

$$\begin{aligned}\mathcal{U}(t_{m+1}) - \mathcal{U}(t_m) &= \frac{1}{\Gamma(\xi)}\int_0^{t_{m+1}} (t_{m+1}-t)^{\xi-1}\mathcal{K}_1(t, \mathcal{U}(t)) + \frac{1}{\Gamma(\xi)}\int_0^{t_m} (t_m-t)^{\xi-1}\mathcal{K}_1(t, \mathcal{U}(t))dt,\\ \mathcal{V}(t_{m+1}) - \mathcal{V}(t_m) &= \frac{1}{\Gamma(\xi)}\int_0^{t_{m+1}} (t_{m+1}-t)^{\xi-1}\mathcal{K}_2(t, \mathcal{V}(t)) + \frac{1}{\Gamma(\xi)}\int_0^{t_m} (t_m-t)^{\xi-1}\mathcal{K}_2(t, \mathcal{V}(t))dt.\end{aligned} \tag{39}$$

Eq. (39) can be expressed in the form of Eq. (34), resulting in

$$\begin{aligned}\mathcal{U}(t_{m+1}) &= \mathcal{U}(t_m) + \frac{g(t_m, \mathcal{U}_m)}{h\Gamma(\xi)}\left\{\frac{2ht_{m+1}^{\xi}}{\xi} - \frac{t_{m+1}^{\xi+1}}{\xi+1} + \frac{ht_m^{\xi}}{\xi} - \frac{t_m^{\xi+1}}{\xi+1}\right\} + \frac{g(t_{m-1}, \mathcal{U}_{m-1})}{h\Gamma(\xi)}\left\{\frac{ht_{m+1}^{\xi}}{\xi} - \frac{t_{m+1}^{\xi+1}}{\xi+1} + \frac{t_m^{\xi}}{\xi+1}\right\},\\ \mathcal{V}(t_{m+1}) &= \mathcal{V}(t_m) + \frac{g(t_m, \mathcal{V}_m)}{h\Gamma(\xi)}\left\{\frac{2ht_{m+1}^{\xi}}{\xi} - \frac{t_{m+1}^{\xi+1}}{\xi+1} + \frac{ht_m^{\xi}}{\xi} - \frac{t_m^{\xi+1}}{\xi+1}\right\} + \frac{g(t_{m-1}, \mathcal{V}_{m-1})}{h\Gamma(\xi)}\left\{\frac{ht_{m+1}^{\xi}}{\xi} - \frac{t_{m+1}^{\xi+1}}{\xi+1} + \frac{t_m^{\xi}}{\xi+1}\right\}.\end{aligned} \tag{40}$$

Based on Theorem 6.1, we derive from Eq. (40)

$$\begin{aligned}\mathcal{U}(t_{m+1}) &= \mathcal{U}(t_m) + \frac{g(t_m, \mathcal{U}_m)}{h\Gamma(\xi)}\left\{\frac{2ht_{m+1}^{\xi}}{\xi} - \frac{t_{m+1}^{\xi+1}}{\xi+1} + \frac{ht_m^{\xi}}{\xi} - \frac{t_m^{\xi+1}}{\xi+1}\right\} + \frac{g(t_{m-1}, \mathcal{U}_{m-1})}{h\Gamma(\xi)}\left\{\frac{ht_{m+1}^{\xi}}{\xi} - \frac{t_{m+1}^{\xi+1}}{\xi+1} + \frac{t_m^{\xi}}{\xi+1}\right\} + {}^1\mathcal{R}_m^{\xi}(t),\\ \mathcal{V}(t_{m+1}) &= \mathcal{V}(t_m) + \frac{g(t_m, \mathcal{V}_m)}{h\Gamma(\xi)}\left\{\frac{2ht_{m+1}^{\xi}}{\xi} - \frac{t_{m+1}^{\xi+1}}{\xi+1} + \frac{ht_m^{\xi}}{\xi} - \frac{t_m^{\xi+1}}{\xi+1}\right\} + \frac{g(t_{m-1}, \mathcal{V}_{m-1})}{h\Gamma(\xi)}\left\{\frac{ht_{m+1}^{\xi}}{\xi} - \frac{t_{m+1}^{\xi+1}}{\xi+1} + \frac{t_m^{\xi}}{\xi+1}\right\} + \mathcal{R}_m^{\xi}(t),\end{aligned}$$

where $\mathcal{R}_m^{\xi}(t) < \frac{h^{3+\xi}M}{12\Gamma(\xi+1)}\{(n+1)^{\xi} + n^2\}, i = 1, 2$.

Numerical simulations of the fractional model

In the first scenario, the demonstration showcases various simulations of the proposed fractional system for various values of the fractional order ξ. Simulations are conducted with parameter values $\alpha = 0.045$, $\beta = 0.045, \Phi = 50.59, \Psi = 100.89, \gamma = 0.045, \delta = 0.45$, $\Lambda = 0.0001$ and $\rho = 0.002$, while the state variables are set as $\mathcal{U}(0) = 200$ and $\mathcal{V}(0) = 100$. We highlight the influence

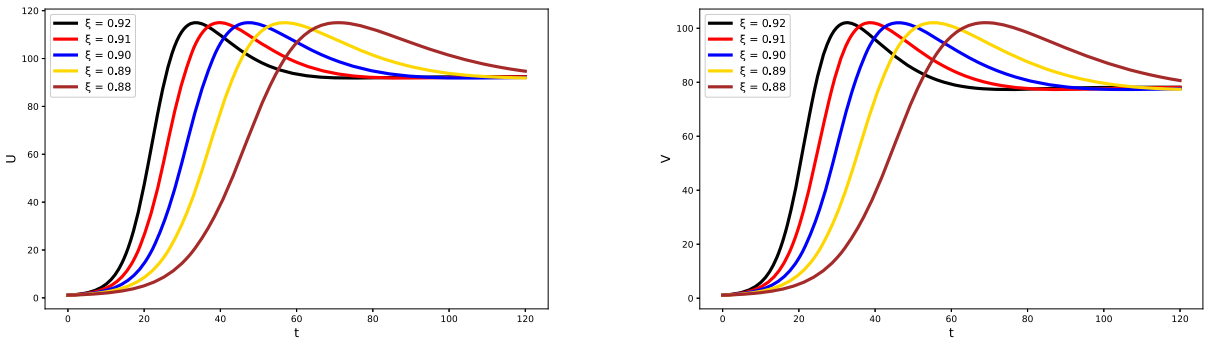

(a) **(b)**

Fig. 1 Dynamics of $\mathcal{U}(t)$ and $\mathcal{V}(t)$ with constraints $\rho < 1$, $\Lambda < 1$, and fractional orders $\xi = 0.92, 0.91, 0.90, 0.89, 0.88$

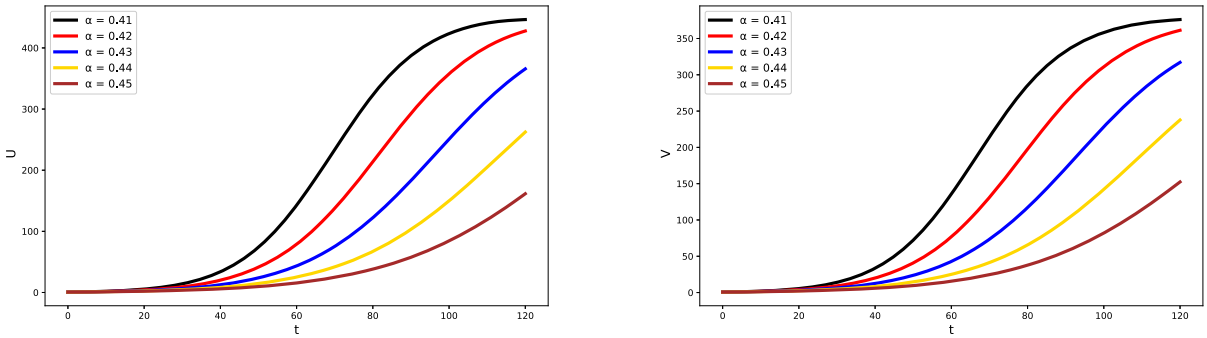

(a) **(b)**

Fig. 2 Variation of α dynamics with $\rho < 1$, $\Lambda = 0$, and fractional orders $\xi = 0.95$

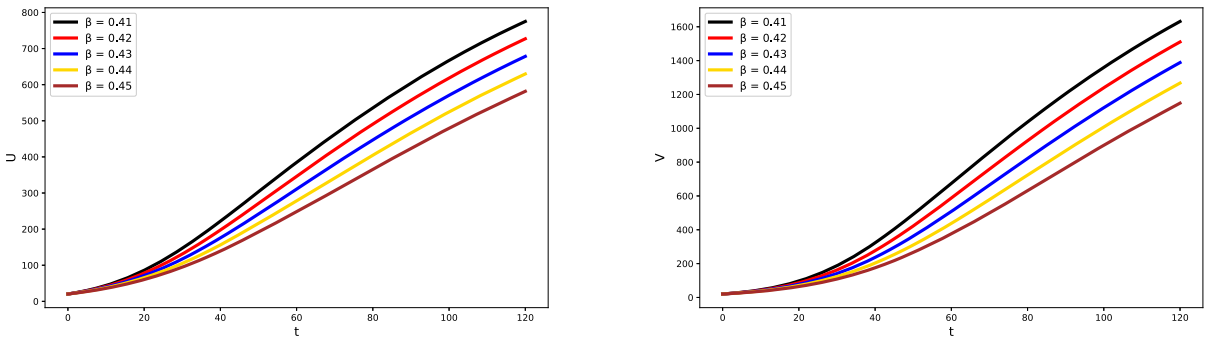

(a) **(b)**

Fig. 3 Variation of β dynamics with $\rho = 0$, $\Lambda < 1$, and fractional orders $\xi = 0.88$

of the fractional order ξ of the Caputo operator exclusively on the dynamics of the model to demonstrate the effect of different parameters. The simulation covers 11 values of

$$\xi : 1, 0.95, 0.92, 0.91, 0.90, 0.89, 0.88, 0.85, 0.83, 0.80, 0.77$$

. The time frame for the simulation is set at 120 days. The results are graphically represented Figs. 1, 2, 3, 4, 5, 6, 7, 8, 9, 10, 11, 12, and 13, showcasing the dynamics of each parameter in the system (6). This confirms the proposed model's capability to accurately simulate the dynamics of the fishery model.

In Fig. 1, population dynamics of unreserved and reserved area with $\rho < 1$, $\Lambda < 1$, and fractional Orders $\xi = 0.92, 0.91, 0.90, 0.89, 0.88$.

In Fig. 2, no harvesting occurs with $\rho < 1$ and $\Lambda = 0$, implying that the fish populations grow naturally, driven

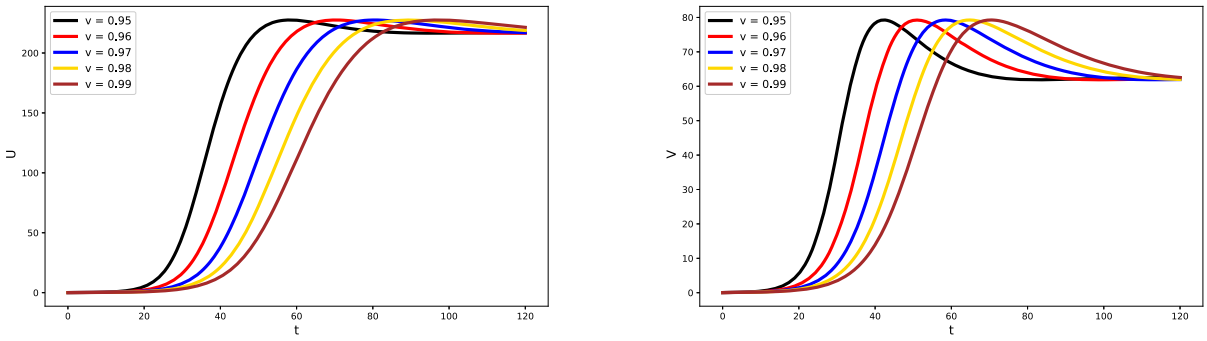

(a) (b)

Fig. 4 Variation of υ dynamics with $\rho < 1$, $\Lambda > 0$, $\gamma = 0.45$ and $\delta > 0$, and fractional orders $\xi = 0.85$

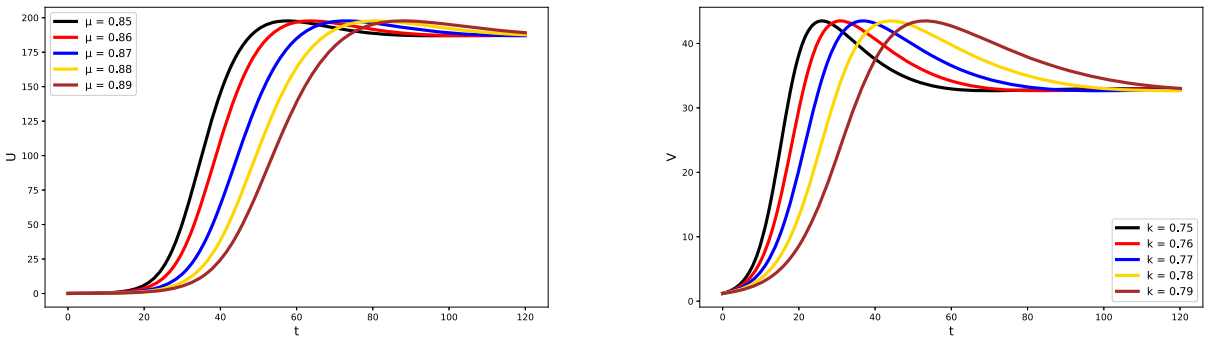

(a) (b)

Fig. 5 Variation of μ dynamics with $\rho < 1$, $\Lambda > 0$, $\gamma = 0.40$ and $\delta > 0$, and fractional orders $\xi = 0.83$

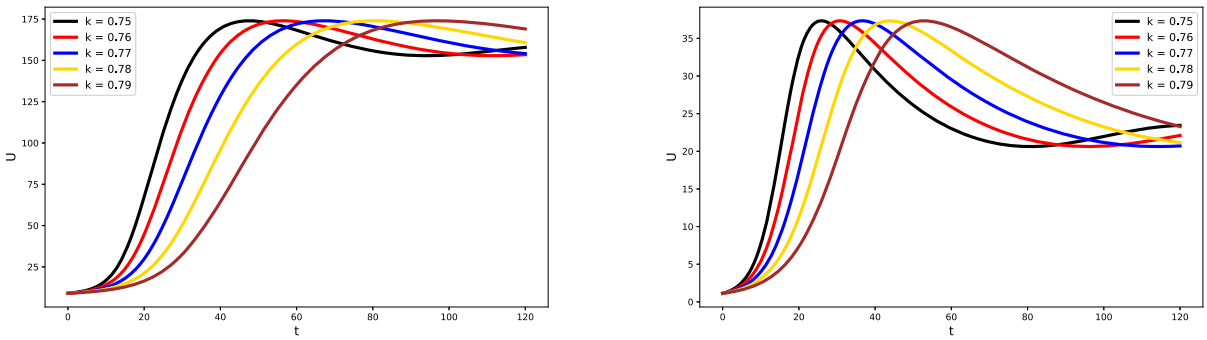

(a) (b)

Fig. 6 Variation of κ dynamics with $\rho < 1$, $\Lambda > 0$, $\gamma > 0$ and $\delta = 0.45$, and fractional orders $\xi = 0.80$

only by the intrinsic growth rate α. As α increases, the fish populations grow faster in unreserved and reserve areas, illustrating how a higher intrinsic growth rate accelerates population recovery without harvesting.

In Fig. 3, $\rho < 1$ and $\Lambda < 1$ show no harvesting, so the intrinsic factors and the $\xi = 0.88$ determine the fish population dynamics. As β increases from 0.41 to 0.45, the growth rate β strengthens, leading to faster population growth. When $\xi = 0.88$, the population dynamics respond more gradually over time; however, when increasing β, the system experiences faster growth.

In Figs. 4, 5, 6, and 7, by increasing parameter values ν, μ, κ and ε, the fish population experiences higher growth rates, as these factors directly enhance the survival and reproduction capabilities of the fish. Adjusting ρ and Λ, particularly by setting $\rho = 0$ and $\Lambda = 0$, means that no

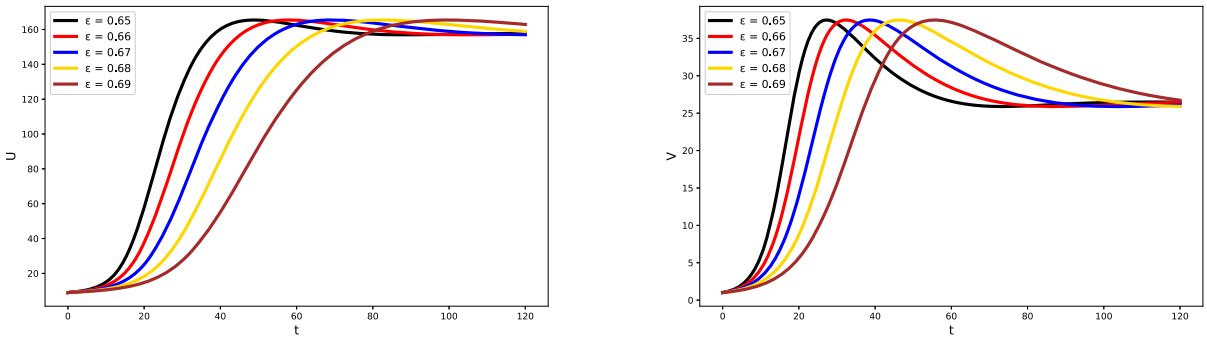

(a) (b)

Fig. 7 Variation of ε dynamics with $\rho < 1$, $\Lambda > 0$, $\gamma > 0$ and $\delta = 0.40$, and fractional orders $\xi = 0.77$

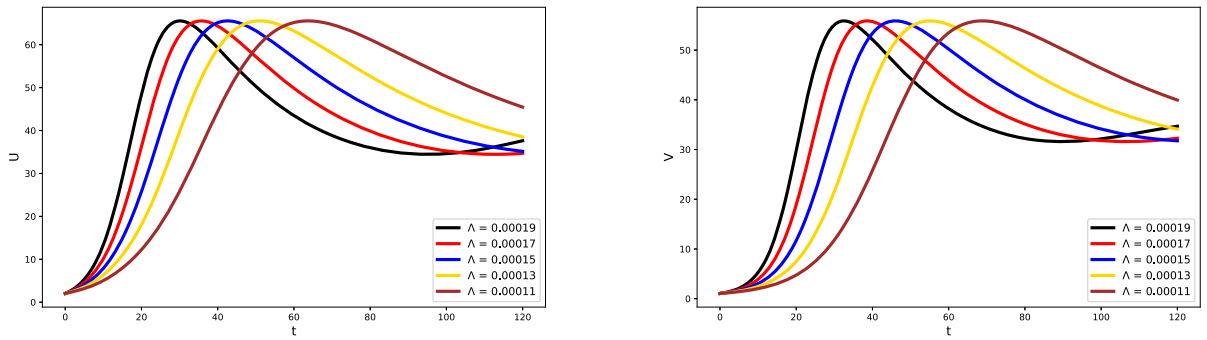

(a) (b)

Fig. 8 Variation of Λ dynamics with $\rho = 0.001$ and fractional orders $\xi = 0.92, 0.91, 0.90, 0.89, 0.88$

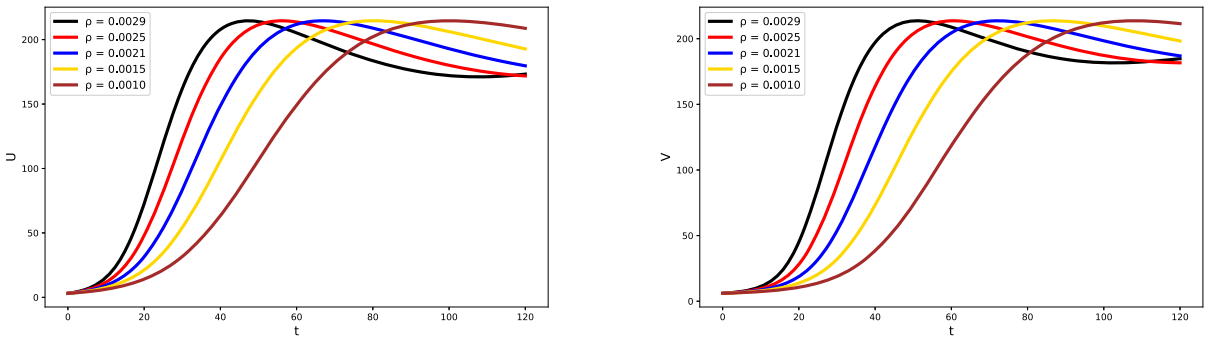

(a) (b)

Fig. 9 Variation of ρ dynamics with $\Lambda = 0.0001$ and fractional orders $\xi = 0.92, 0.91, 0.90, 0.89, 0.88$

harvesting occurs, allowing the population to grow freely. As the fractional order ξ decreases from 0.85 to 0.77, the system shows more memory effect, meaning the population responds more gradually to changes, but with improved conditions (higher values of $\nu, \mu, \kappa, \varepsilon$), the fish population can still experience faster and sustained growth, leading to higher population levels over time.

In Fig. 8, as the harvesting threshold Λ decreases from 0.00019 to 0.00011, the harvesting intensity is reduced, but with $\rho = 0.0001$, the catchability is extremely low, meaning almost no fish are being harvested. Additionally, as the fractional order ξ decreases from 0.92 to 0.88, the system introduces more memory effects, slowing down the fish population's response to environmental changes. The combination of a very low catchability ρ, a decreasing Λ,

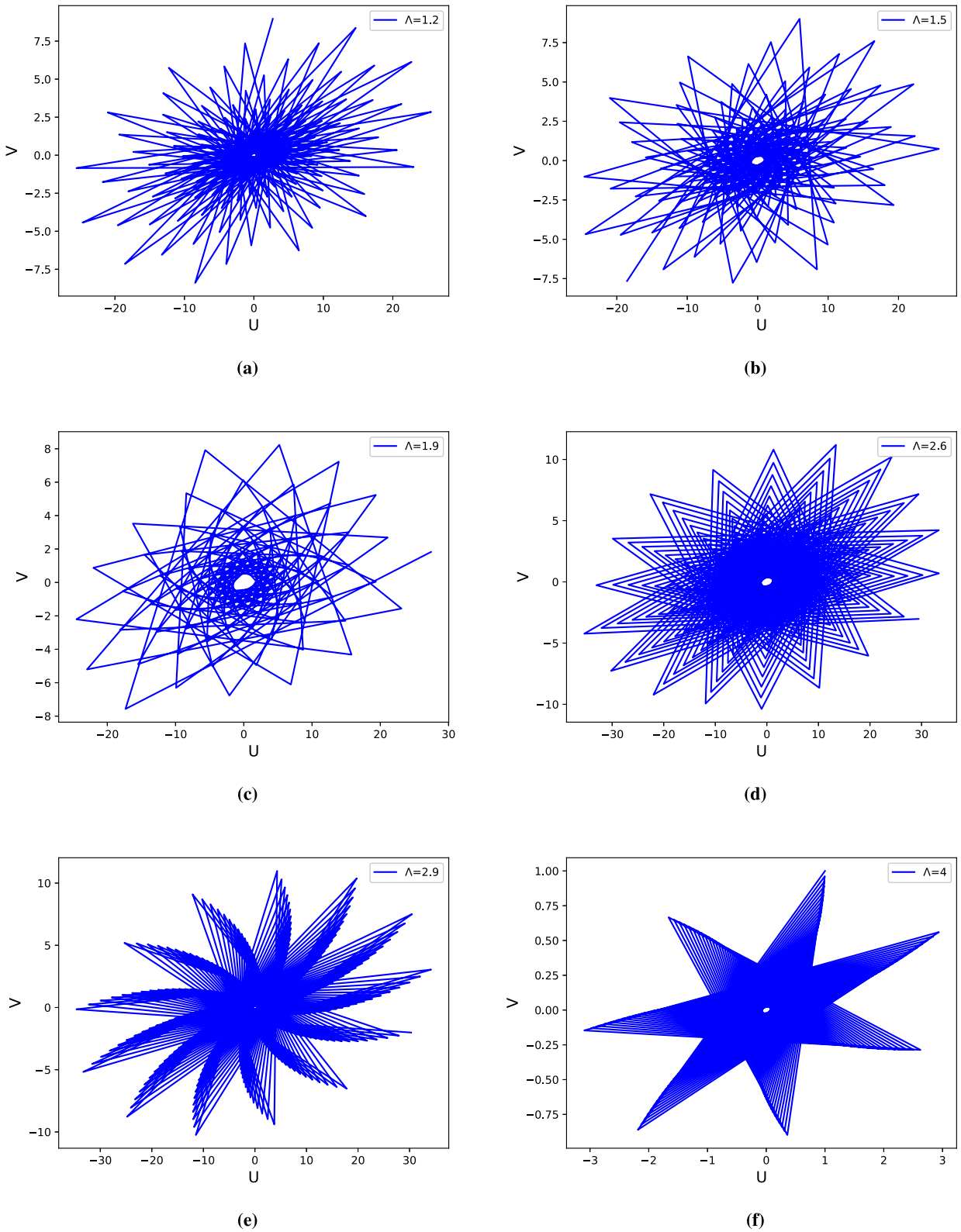

Fig. 10 Dynamics to depict chaotic patterns of the system (6) for varying initial conditions and $\Lambda(1.2, 1.5, 1.9, 2.6, 2.9, 4)$, $\rho > 1$, observed with fractional order $\xi = 0.5$

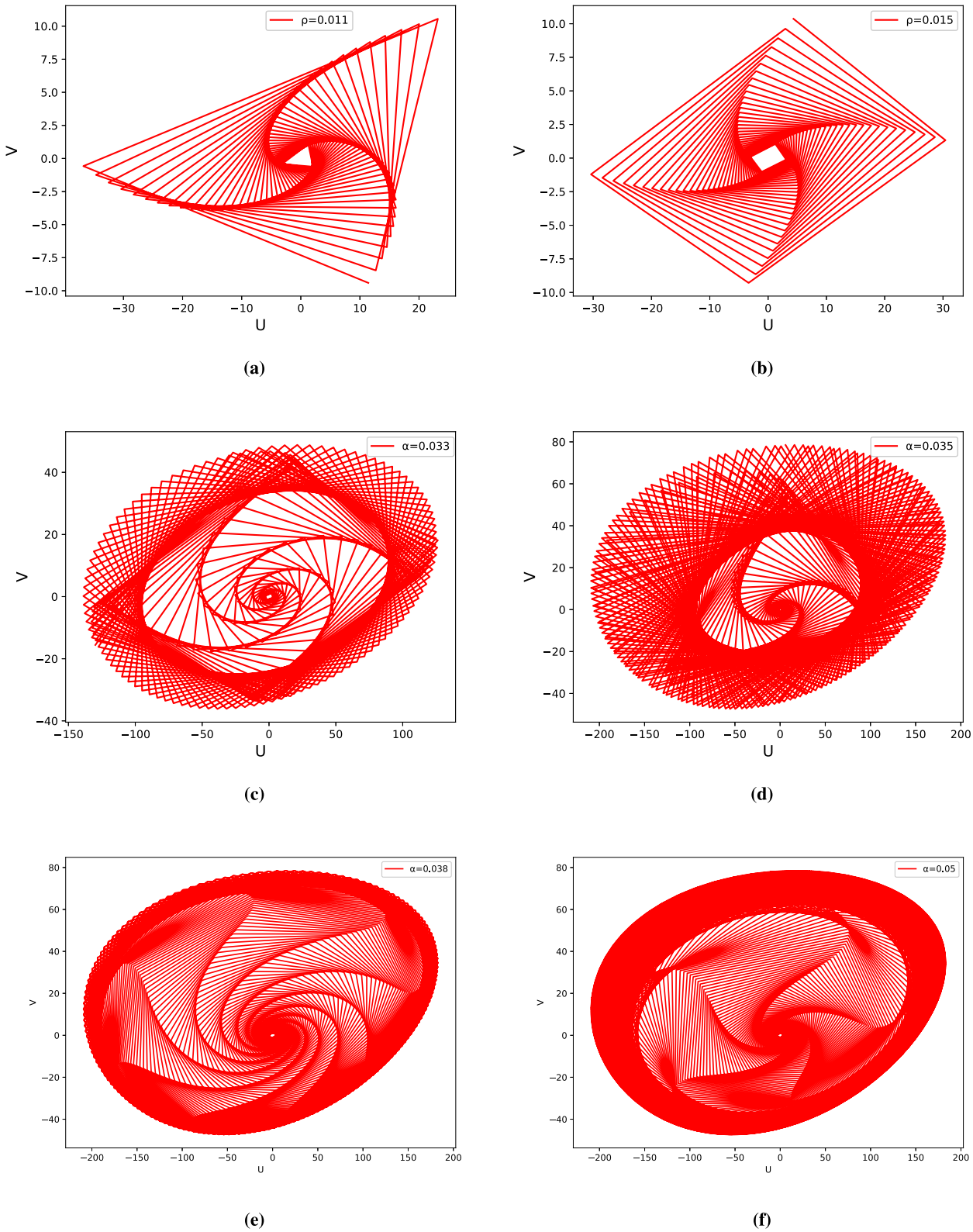

Fig. 11 Dynamics to depict chaotic patterns of the system (6) for varying initial conditions and $\rho, \alpha, \Lambda > 1$, observed with fractional order $\xi = 0.41$

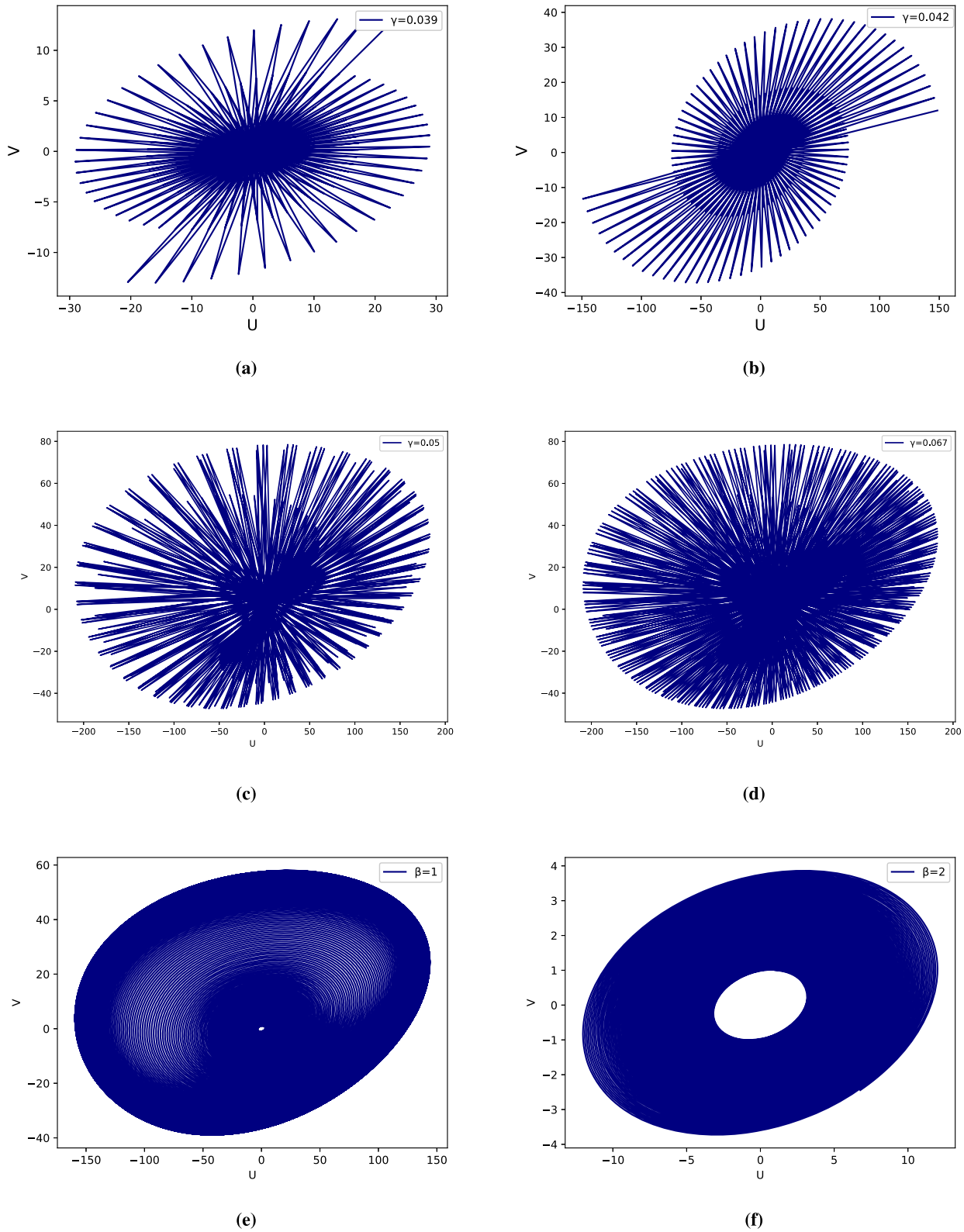

Fig. 12 Dynamics to depict chaotic patterns of the system (6) for varying initial conditions and $\gamma, \beta, \rho, \Lambda > 1$, observed with fractional order $\xi = 0.35$

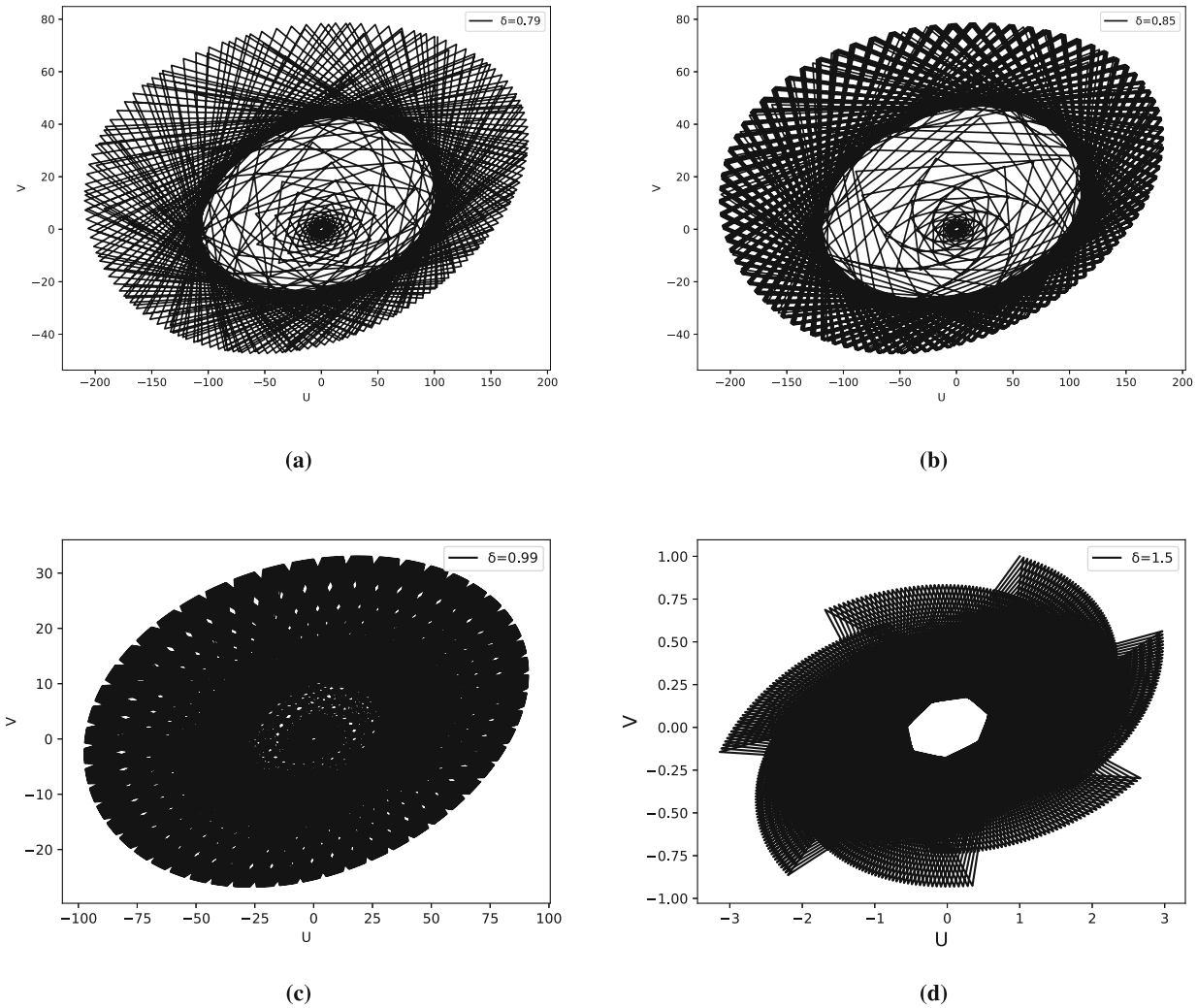

Fig. 13 Dynamics to depict chaotic patterns of the system (6) for varying initial conditions and δ, $\rho, \Lambda > 1$, observed with fractional order $\xi = 0.2$

and a decreasing ξ results in a situation where the fish population experiences gradual growth or stabilization due to minimal harvesting pressure and slower but sustained responses influenced by the fractional order model.

In Fig. 9, harvesting efficiency is significantly reduced as the catchability coefficient ρ decreases from 0.0029 to 0.001. With $\Lambda = 0.0001$, the harvesting threshold is extremely low, preventing substantial harvesting activity. Additionally, as the fractional order ξ decreases from 0.92 to 0.88, the system exhibits more memory effects, causing the fish population to respond more gradually to changes over time.

Thus, this combination of lower catchability ρ, minimal harvesting threshold Λ, and a decreasing fractional order ξ results in a situation where the fish population is largely unaffected by harvesting and grows more slowly but steadily. The decreasing ξ introduces a more gradual population response, but overall, the system favours population stability and growth due to the minimal impact of harvesting. Figures 10, 11, 12, and 13 chaotic behaviour arises due to the interactions between high harvesting intensity Λ, low catchability ρ, slow growth rate, and the integer-order dynamics of the system. The chaotic behavior of our system for varying the parameters $\alpha, \beta, \gamma, \delta$ and memory indices ξ. These memory indices are also effective control parameters for causing chaos in a system. This insight is particularly important for applications that rely on chaotic behavior, as chaos has a significant role in many fields, including scientific and engineering. Chaotic modeling demonstrates the feasibility and scalability of the proposed mathematical model, suggesting its potential application to novel chaotic systems. We further highlight the substantial contribution of the parameters, which may serve as effective tools for implementing preventive actions within such systems.

Conclusion

This study examined a fishery model initially constructed as an integer-order nonlinear system comprising two differential equations. Recognizing the importance of the fractional modeling method, we seamlessly extended to fractional order via the well-known Caputo operator. Our study included detailed fundamental aspects such as boundary, positivity analysis, and existence and uniqueness in the model's fractional order and stability analysis. Our investigations illuminated the profound influence of varying ρ and Λ, consequentially witnessing a commensurate rise in population dynamics on the fishery model. Adjusting the key parameters ρ and Λ allowed a detailed exploration of population growth and stability under various harvesting scenarios. The model effectively captures the memory effects and gradual responses within the fishery model's population dynamics by incorporating fractional-order derivatives. Using the Caputo fractional derivative, a new numerical scheme is presented to conceptualize the dynamics fishry model and chaotic plots are presented with different parameter adjustments. This illustrates Caputo Adam–Bashforth's effectiveness in grasping and comprehending fractional-order dynamics in ecological models to capture complex dynamics, offering a more accurate and flexible numerical solution and valuable insights into long-term behavior. These simulations illustrated the effects of various parameters and fractional orders of the Caputo operator, providing a valuable tool for simulating and understanding ecological models with fractional order. To improve the robustness of the chaotic behavior, alternative fractional operators will be considered in future work, including the Caputo–Fabrizio and the Atangana–Baleanu derivatives.

Acknowledgements Prince Sultan University is appreciated for support through TAS research lab.

Author contributions The first three authors wrote the paper. K.S edited the paper. B.A and T.A revised the last version.

Funding Open access funding provided by Sefako Makgatho Health Sciences University. No external source of funding exists.

Data availability No datasets were generated or analysed during the current study.

Declarations

Conflict of interest The authors declare no competing interests.

References

Adel W, Günerhan H, Nisar KS, Agarwal P, El-Mesady A (2024) Designing a novel fractional order mathematical model for COVID-19 incorporating lockdown measures. Sci Rep 14:2926

Ali A, Ansari KJ, Alrabaiah H, Aloqaily A, Mlaiki N (2023) Coupled system of fractional impulsive problem involving power–law kernel with piecewise order. Fract Fraction 7(6):436

Biswas MHA, Hossain MR, Mondal MK (2017) Mathematical modeling applied to sustainable management of marine resources. Proc Eng 194:337–344

Broadbridge P, Hutchinson AJ, Li X, Mann BQ (2022) Stratified mobility fishery models with harvesting outside of no-take areas. Appl Math Model 105:29–49

Buxton CD, Hartmann K, Kearney R, Gardner C (2014) When is spillover from marine reserves likely to benefit fisheries? PLoS ONE 9(9):e107032

Dasumani M, Moore SE, Gathungu DK, Diallo B (2024) A nonlinear fractional fishery resource system model with Crowley–Martin functional response under Mittag–Leffler kernel. Results Control Optim 16:100461

Dasumani M, Lassong BS, Akgül A, Osman S, Moore SE (2024) Analyzing the dynamics of human papillomavirus transmission via fractal and fractional dimensions under Mittag–Leffler law. Model Earth Syst Environ 10:7225–7249

Diallo B, Dasumani M, Okelo JA, Osman S, Sow O, Aguegboh NS, Okongo W (2025) Fractional optimal control problem modeling bovine tuberculosis and rabies co-infection. Results Control Optim 18:100523

Gerber LR, Botsford LW, Hastings A, Possingham HP, Gaines SD, Palumbi SR, Andelman S (2003) Population models for marine reserve design: a retrospective and prospective synthesis. Ecol Appl 13(sp1):47–64

Grüss A (2014) Modelling the impacts of marine protected areas for mobile exploited fish populations and their fisheries: what we recently learnt and where we should be going. Aquat Liv Resour 27(3–4):107–133

Khan NA, Razzaq OA, Mondal SP, Rubbab Q (2019) Fractional order ecological system for complexities of interacting species with harvesting threshold in imprecise environment. Adv Differ Equ 2019:1–34

Khan H, Alzabut J, Shah A, He ZY, Etemad S, Rezapour S, Zada A (2023) On fractal-fractional waterborne disease model: A study on theoretical and numerical aspects of solutions via simulations. Fractals 31(04):2340055

Khan H, Aslam M, Rajpar AH, Chu YM, Etemad S, Rezapour S, Ahmad H (2024) A new fractal-fractional hybrid model for studying climate change on coastal ecosystems from the mathematical point of view. Fractals 32(02):2440015

Lassong BS, Dasumani M, Mung'atu JK, Moore SE (2024) Power and Mittag–Leffler laws for examining the dynamics of fractional unemployment model: a comparative analysis. Chaos Solitons Fract X 13:100117

Li C, Qian D, Chen Y (2011) On Riemann–Liouville and Caputo derivatives. Discret Dyn Nat Soc 2011(1):562494

Li X, Xu Q, Xia R, Zhang N, Wang S, Ding S, Chen X (2024) Stochastic process is main factor to affect plateau river fish community assembly. Environ Res 254:119083

Mahmoud EE, Trikha P, Jahanzaib LS, Almaghrabi OA (2020) Dynamical analysis and chaos control of the fractional chaotic ecological model. Chaos Solitons Fract 141:110348

Maiti AP, Dubey B (2017) Stability and bifurcation of a fishery model with Crowley–Martin functional response. Int J Bifurc Chaos 27(11):1750174

Maurya J, Misra AK, Banerjee S (2025) Bifurcation analysis of fish-algae-nutrient interactions in aquatic ecosystems. Nonlinear Dyn 113(2):1713–1743

McClanahan TR, Muthiga NA, Coleman RA (2011) Testing for top-down control: can post-disturbance fisheries closures reverse algal dominance? Aquat Conserv Mar Freshwat Ecosyst 21(7):658–675

Milici C, Draganescu G, Machado JT (2018) Introduction to fractional differential equations, vol 25. Springer, Berlin

Paul S, Mahata A, Mukherjee S, Mali PC, Roy B (2023a) Fractional order SEIQRD epidemic model of Covid-19: a case study of Italy. PLoS ONE 18(3):e0278880

Paul S, Mahata A, Mukherjee S, Mahato SK, Salimi M, Roy B (2023b) Study of fuzzy fractional Caputo order approach to diabetes model. Fuzzy optimization, decision-making and operations research: theory and applications. Springer International Publishing, New York, Cham, pp 423–434

Paul S, Mahata A, Karak M, Mukherjee S, Biswas S, Roy B (2024) Dynamical behavior of fractal–fractional order monkeypox virus model. Franklin Open 7:100103

Paul S, Mahata A, Karak M, Mukherjee S, Biswas S, Roy B (2024) A fractal-fractional order susceptible-exposed-infected-recovered (SEIR) model with Caputo sense. Healthc Anal 5:100317

Podlubny I (1999) An introduction to fractional derivatives, fractional differential equations, to methods of their solution and some of their applications. Math Sci Eng 198:340

Wang Z (2013) A numerical method for delayed fractional-order differential equations. J Appl Math 2013(1):256071

Weigel JY, Mannle KO, Bennett NJ, Carter E, Westlund L, Burgener V, Hellman A (2014) Marine protected areas and fisheries: bridging the divide. Aquat Conserv Mar Freshw Ecosyst 24(S2):199–215

Yadav S, Pandey RK, Shukla AK (2019) Numerical approximations of Atangana–Baleanu Caputo derivative and its application. Chaos Solitons Fract 118:58–64

Yoshioka H (2025) Superposition of interacting stochastic processes with memory and its application to migrating fish counts. Chaos Solitons Fract 192:115911